Shell-model-like approach based on cranking covariant density functional theory: Band crossing and shape evolution in ^{60}Fe

Z. Shi (施智),[1] Z. H. Zhang (张振华),[2] Q. B. Chen (陈启博),[3,4] S. Q. Zhang (张双全),[3,*] and J. Meng (孟杰)[3,1,5,†]

[1]*School of Physics and Nuclear Energy Engineering, Beihang University, Beijing 100191, China*
[2]*Mathematics and Physics Department, North China Electric Power University, Beijing 102206, China*
[3]*State Key Laboratory of Nuclear Physics and Technology, School of Physics, Peking University, Beijing 100871, China*
[4]*Physik-Department, Technische Universität München, D-85747 Garching, Germany*
[5]*Yukawa Institute for Theoretical Physics, Kyoto University, Kyoto 606-8502, Japan*

(Received 16 January 2018; published 20 March 2018)

The shell-model-like approach is implemented to treat the cranking many-body Hamiltonian based on the covariant density functional theory including pairing correlations with exact particle number conservation. The self-consistency is achieved by iterating the single-particle occupation probabilities back to the densities and currents. As an example, the rotational structures observed in the neutron-rich nucleus ^{60}Fe are investigated and analyzed. Without introducing any *ad hoc* parameters, the bandheads, the rotational spectra, and the relations between the angular momentum and rotational frequency for the positive-parity band A and negative-parity bands B and C are well reproduced. The essential role of the pairing correlations is revealed. It is found that for band A, the band crossing is due to the change of the last two occupied neutrons from the $1f_{5/2}$ signature partners to the $1g_{9/2}$ signature partners. For the two negative-parity signature partner bands B and C, the band crossings are due to the pseudocrossing between the $1f_{7/2,5/2}$ and the $1f_{5/2,1/2}$ orbitals. Generally speaking, the deformation parameters β for bands A, B, and C decrease with rotational frequency. For band A, the deformation jumps from $\beta \approx 0.19$ to $\beta \approx 0.29$ around the band crossing. In comparison with its signature partner band C, band B exhibits appreciable triaxial deformation.

DOI: 10.1103/PhysRevC.97.034317

I. INTRODUCTION

In recent decades, lots of novel phenomena with unexpected features in nuclear structure, including superdeformed rotational bands [1,2], neutron halos [3,4] and giant halos [5–7], the disappearance and occurrence of magic numbers [8], magnetic and antimagnetic rotation [9–12], chiral doublet bands [13,14], and multiple chiral doublets (MχD) [15–18], have attracted worldwide attention and challenged nuclear models aiming at a unified and microscopic interpretation of these phenomena.

Starting from an effective nucleon-nucleon interaction with Lorentz invariance, the covariant density functional theory (CDFT) naturally includes the spin-orbit coupling and has achieved great successes in describing many nuclear phenomena in stable and exotic nuclei of the whole nuclear chart [2,6,7,19,20]. Based on the same functional and without introducing any additional parameters, the CDFT can well describe the rotational excitations in nuclei by including the cranking terms [12,21,22]. Up to now, the cranking CDFT has been developed for the principal axis cranking (PAC) [23], the tilted axis cranking (TAC) [24,25], and also the aplanar TAC [22,26]. With various versions of cranking CDFT, novel rotational phenomena including superdeformed rotational bands [23,27,28], magnetic [22,24,25,29] and antimagnetic rotation [30,31], linear cluster structure [32], and chiral doublet bands [26] have been investigated successfully.

Pairing correlations are essential to describe not only the nuclear ground-state properties [20,33,34] but also the excited-state properties [20,35–38]. Within the mean-field approximation, the pairing correlations are usually treated by the Bardeen-Cooper-Schrieffer (BCS) approximation or Bogoliubov transformation [34]. However, the particle number is not conserved in the standard BCS and Bogoliubov approximations. The blocking effect, which is responsible for various odd-even differences in nuclear properties and important for low-lying excited states, can only be approximately considered. Another difficulty is the pairing collapse with rotation [39]. Moreover, the BCS approximation can not be applied to the cranking model as the time-reversal symmetry is broken. Although these defects can be remedied by the particle number projection technique [34,40–43], the calculation algorithm is complicated and the simplicity is lost [34].

Shell-model-like approach (SLAP) [44], originally referred to as the particle-number-conserving (PNC) method [45], treats pairing correlations and blocking effects exactly by diagonalizing the many-body Hamiltonian in a many-particle configuration (MPC) space with conserved particle number. Based on the phenomenological cranking Nilsson model, extensive applications for the odd-even differences in moments of inertia [46], identical bands [47,48], nuclear pairing phase transition [49], antimagnetic rotation [50,51], and high-K rotational bands in the rare-earth [52–58] and actinide [59–61]

*sqzhang@pku.edu.cn
†mengj@pku.edu.cn

nuclei, have been performed. Furthermore, the SLAP has been combined with CDFT [44,62], deformed Woods-Saxon potential [63,64], and the Skyrme density functional [65,66]. Similar approaches to treat pairing correlations with conserved particle number can be found in Refs. [67–72]. Based on the CDFT, the SLAP has been first adopted to study the ground-state properties and low-lying excited states for Ne isotopes [44]. In Ref. [62], the extension to include the temperature has been implemented to study the heat capacity.

In this paper, the SLAP is implemented to treat the cranking many-body Hamiltonian based on the CDFT including pairing correlations with exact particle number conservation and is referred to as cranking CDFT-SLAP. Our aim is to investigate the rotational excitation modes of superfluid nuclei in a fully microscopic, self-consistent, and particle-number-conserved manner. As an example, the rotational spectra in the neutron-rich nucleus ^{60}Fe will be investigated with one of the most successful functionals PC-PK1 [31]. Being a key isotope in astrophysics and cosmic nucleosynthesis, the low-lying structure and rotational spectra in ^{60}Fe have been investigated experimentally [73–76] and theoretically with the projected shell model [77] and the large-scale shell model [78].

The paper is organized as follows. In Sec. II, the theoretical frameworks for the cranking CDFT and the SLAP are briefly presented. The numerical details are given in Sec. III. In Sec. IV, the energy spectra and the relations between total angular momenta and rotational frequency for the three rotational bands in ^{60}Fe calculated by the cranking CDFT-SLAP are presented and compared with the data. The band-crossing mechanisms and shape evolutions in these rotational bands are discussed. A short summary is given in Sec. V.

II. THEORETICAL FRAMEWORK

A. Cranking covariant density functional theory

The effective Lagrangian density for the point-coupling covariant density functional is as follows [31,79]:

$$\begin{aligned}\mathcal{L} &= \mathcal{L}^{\text{free}} + \mathcal{L}^{\text{4f}} + \mathcal{L}^{\text{hot}} + \mathcal{L}^{\text{der}} + \mathcal{L}^{\text{em}} \\ &= \bar{\psi}(i\gamma_\mu\partial^\mu - m)\psi - \frac{1}{2}\alpha_S(\bar{\psi}\psi)(\bar{\psi}\psi) \\ &\quad - \frac{1}{2}\alpha_V(\bar{\psi}\gamma_\mu\psi)(\bar{\psi}\gamma^\mu\psi) - \frac{1}{2}\alpha_{TV}(\bar{\psi}\vec{\tau}\gamma_\mu\psi)(\bar{\psi}\vec{\tau}\gamma^\mu\psi) \\ &\quad - \frac{1}{3}\beta_S(\bar{\psi}\psi)^3 - \frac{1}{4}\gamma_S(\bar{\psi}\psi)^4 - \frac{1}{4}\gamma_V[(\bar{\psi}\gamma_\mu\psi)(\bar{\psi}\gamma^\mu\psi)]^2 \\ &\quad - \frac{1}{2}\delta_S\partial_\nu(\bar{\psi}\psi)\partial^\nu(\bar{\psi}\psi) - \frac{1}{2}\delta_V\partial_\nu(\bar{\psi}\gamma_\mu\psi)\partial^\nu(\bar{\psi}\gamma^\mu\psi) \\ &\quad - \frac{1}{2}\delta_{TV}\partial_\nu(\bar{\psi}\vec{\tau}\gamma_\mu\psi)\partial^\nu(\bar{\psi}\vec{\tau}\gamma^\mu\psi) \\ &\quad - \frac{1}{4}F^{\mu\nu}F_{\mu\nu} - e\frac{1-\tau_3}{2}\bar{\psi}\gamma^\mu\psi A_\mu, \end{aligned} \tag{1}$$

which includes the free nucleon term $\mathcal{L}^{\text{free}}$, the four-fermion point-coupling terms $\mathcal{L}^{\text{4f}}$, the higher order terms $\mathcal{L}^{\text{hot}}$ responsible for the medium effects, the gradient terms $\mathcal{L}^{\text{der}}$ simulating the effects of finite range, and the electromagnetic interaction terms $\mathcal{L}^{\text{em}}$.

To describe the nuclear rotation, the effective Lagrangian (1) is transformed into a rotating frame with a constant rotational frequency ω_x around the x axis [21,27,80]. The equation of motion for the nucleons derived from the rotating Lagrangian is written as

$$\hat{h}_0\psi_\mu = (\hat{h}_{\text{s.p.}} + \hat{h}_{\text{c}})\psi_\mu = \varepsilon_\mu\psi_\mu, \tag{2}$$

with

$$\hat{h}_{\text{s.p.}} = \boldsymbol{\alpha}\cdot(-i\boldsymbol{\nabla} - \boldsymbol{V}) + \beta(m+S) + V^0, \quad \hat{h}_{\text{c}} = -\omega_x\cdot\hat{j}_x, \tag{3}$$

where $\hat{j}_x = \hat{l}_x + \frac{1}{2}\Sigma_x$ is the x component of the total angular momentum of the nucleon spinors and ε_μ represents the single-particle Routhians for nucleons. The relativistic fields $S(\boldsymbol{r})$ and $V^\mu(\boldsymbol{r})$ have the form

$$\begin{aligned} S(\boldsymbol{r}) &= \alpha_S\rho_S + \beta_S\rho_S^2 + \gamma_S\rho_S^3 + \delta_S\Delta\rho_S, \\ V^0(\boldsymbol{r}) &= \alpha_V\rho_V + \gamma_V\rho_V^3 + \delta_V\Delta\rho_V + \tau_3\alpha_{TV}\rho_{TV} \\ &\quad + \tau_3\delta_{TV}\Delta\rho_{TV} + e\frac{1-\tau_3}{2}A^0, \\ \boldsymbol{V}(\boldsymbol{r}) &= \alpha_V\boldsymbol{j}_V + \gamma_V(\boldsymbol{j}_V)^3 + \delta_V\Delta\boldsymbol{j}_V \\ &\quad + \tau_3\alpha_{TV}\boldsymbol{j}_{TV} + \tau_3\delta_{TV}\Delta\boldsymbol{j}_{TV} + e\frac{1-\tau_3}{2}\boldsymbol{A}, \end{aligned} \tag{4}$$

with ρ and $\boldsymbol{j}$ respectively represent the local densities and currents,

$$\begin{aligned} \rho_S(\boldsymbol{r}) &= \sum_\mu n_\mu\bar{\psi}_\mu(\boldsymbol{r})\psi_\mu(\boldsymbol{r}), \\ \rho_V(\boldsymbol{r}) &= \sum_\mu n_\mu\psi_\mu^\dagger(\boldsymbol{r})\psi_\mu(\boldsymbol{r}), \\ \boldsymbol{j}_V(\boldsymbol{r}) &= \sum_\mu n_\mu\psi_\mu^\dagger(\boldsymbol{r})\boldsymbol{\alpha}\psi_\mu(\boldsymbol{r}), \\ \rho_{TV}(\boldsymbol{r}) &= \sum_\mu n_\mu\psi_\mu^\dagger(\boldsymbol{r})\boldsymbol{\tau}_3\psi_\mu(\boldsymbol{r}), \\ \boldsymbol{j}_{TV}(\boldsymbol{r}) &= \sum_\mu n_\mu\psi_\mu^\dagger(\boldsymbol{r})\boldsymbol{\alpha}\tau_3\psi_\mu(\boldsymbol{r}), \\ \rho_c(\boldsymbol{r}) &= \sum_\mu n_\mu\psi_\mu^\dagger(\boldsymbol{r})\frac{1-\tau_3}{2}\psi_\mu(\boldsymbol{r}), \end{aligned} \tag{5}$$

in which n_μ is the occupation probability for each state μ. The sums are taken over the states with positive energies only, i.e., the contributions of the negative-energy states are neglected (no-sea approximation). It is noted that the spatial components of the electromagnetic vector potential $\boldsymbol{A}$ are neglected since their contributions are extremely small.

After solving the equation of motion (2) self-consistently, the total energy of the system in the laboratory is obtained as

$$E_{\text{tot}} = E_{\text{kin}} + E_{\text{int}} + E_{\text{cou}} + E_{\text{c.m.}}, \tag{6}$$

with the energies of kinetic part,

$$E_{\text{kin}} = \int d^3\boldsymbol{r}\sum_\mu n_\mu\psi_\mu^\dagger[\boldsymbol{\alpha}\cdot\boldsymbol{p} + \beta m]\psi_\mu, \tag{7}$$

the interaction part,

$$E_{\rm int} = \int d^3\boldsymbol{r}\Big\{\frac{1}{2}\alpha_S\rho_S^2 + \frac{1}{3}\beta_S\rho_S^3 + \frac{1}{4}\gamma_S\rho_S^4 + \frac{1}{2}\delta_S\rho_S\Delta\rho_S + \frac{1}{2}\alpha_V\big(\rho_V^2 - \boldsymbol{j}\cdot\boldsymbol{j}\big) + \frac{1}{2}\alpha_{TV}\big(\rho_{TV}^2 - \boldsymbol{j}_{TV}\cdot\boldsymbol{j}_{TV}\big) + \frac{1}{4}\gamma_V\big(\rho_V^2 - \boldsymbol{j}\cdot\boldsymbol{j}\big)^2 + \frac{1}{2}\delta_V(\rho_V\Delta\rho_V - \boldsymbol{j}\Delta\boldsymbol{j}) + \frac{1}{2}\delta_{TV}(\rho_{TV}\Delta\rho_{TV} - \boldsymbol{j}_{TV}\Delta\boldsymbol{j}_{TV})\Big\}, \tag{8}$$

the electromagnetic part,

$$E_{\rm cou} = \int d^3\boldsymbol{r}\frac{1}{2}eA_0\rho_c, \tag{9}$$

and the center-of-mass (c.m.) correction part,

$$E_{\rm c.m.} = -\frac{\langle\hat{\boldsymbol{P}}_{\rm c.m.}^2\rangle}{2mA}, \tag{10}$$

with the mass number A and the total momentum in the center-of-mass frame $\hat{\boldsymbol{P}}_{\rm c.m.} = \sum_i \hat{\boldsymbol{p}}_i$.

The Dirac equation (2) can be solved by expanding the nucleon spinors in a complete set of basis states. In the present work, the three-dimensional harmonic oscillator (3DHO) bases in Cartesian coordinates [24,81–84] with good signature quantum number are adopted,

$$\Phi_{\xi+}(\boldsymbol{r},\boldsymbol{s}) = \langle\boldsymbol{r},\boldsymbol{s}|\xi\alpha = +\rangle = \phi_{n_x}\phi_{n_y}\phi_{n_z}\frac{i^{n_y}}{\sqrt{2}}(-1)^{n_z+1}\begin{pmatrix}1\\(-1)^{n_y+n_z}\end{pmatrix}, \tag{11}$$

$$\Phi_{\xi-}(\boldsymbol{r},\boldsymbol{s}) = \langle\boldsymbol{r},\boldsymbol{s}|\xi\alpha = -\rangle = \phi_{n_x}\phi_{n_y}\phi_{n_z}\frac{i^{n_y}}{\sqrt{2}}\begin{pmatrix}1\\(-1)^{n_y+n_z+1}\end{pmatrix}, \tag{12}$$

which correspond to the eigenfunctions of the signature operation with the positive ($\alpha = +1/2$) and negative ($\alpha = -1/2$) eigenvalues, respectively. The n_x, n_y, and n_z are the harmonic oscillator quantum numbers in x, y, and z directions and ϕ_{n_x}, ϕ_{n_y}, and ϕ_{n_z} are the corresponding eigenstates. The phase factor i^{n_y} is added in order to get real matrix elements for the Dirac equation [12]. Furthermore, under the time-reversal operation $\hat{\mathcal{T}} = -i\sigma_y\hat{K}$, these 3DHO bases the following properties:

$$\hat{\mathcal{T}}\Phi_{\xi+}(\boldsymbol{r},\boldsymbol{s}) = \Phi_{\xi-}(\boldsymbol{r},\boldsymbol{s}), \quad \hat{\mathcal{T}}\Phi_{\xi-}(\boldsymbol{r},\boldsymbol{s}) = -\Phi_{\xi+}(\boldsymbol{r},\boldsymbol{s}). \tag{13}$$

It means that under a proper phase factor, the $\Phi_{\xi+}$ and $\Phi_{\xi-}$ are a pair of time-reversal states with the same quantum numbers n_x, n_y, and n_z.

B. Shell-model-like approach

The cranking many-body Hamiltonian with pairing correlations reads

$$\hat{H} = \hat{H}_0 + \hat{H}_{\rm pair}. \tag{14}$$

The one-body Hamiltonian $\hat{H}_0 = \sum\hat{h}_0$ with $\hat{h}_0$ given in Eq. (2). The monopole pairing Hamiltonian $\hat{H}_{\rm pair}$ is used,

$$\hat{H}_{\rm pair} = -G\sum_{\xi,\eta>0}^{\xi\neq\eta}\hat{\beta}_\xi^\dagger\hat{\beta}_{\bar{\xi}}^\dagger\hat{\beta}_{\bar{\eta}}\hat{\beta}_\eta, \tag{15}$$

where G is the effective pairing strength, $\bar{\xi}$ ($\bar{\eta}$) labels the time-reversal state of ξ (η), and $\xi \neq \eta$ means that the self-scattering for the nucleon pairs is forbidden [44].

The one-body Hamiltonian $\hat{H}_0$ in the 3DHO bases (11) and (12) can be written as

$$\hat{H}_0 = \sum_{\xi\eta,\alpha}h_{\xi\alpha,\eta\alpha}\hat{\beta}_{\xi\alpha}^\dagger\hat{\beta}_{\eta\alpha}. \tag{16}$$

Here $h_{\xi\alpha,\eta\alpha}$ is the matrix element of $\hat{h}_0$ between states $|\xi\alpha\rangle$ and $|\eta\alpha\rangle$. Accordingly, the pairing Hamiltonian $\hat{H}_{\rm pair}$ in the 3DHO bases can be written as

$$\hat{H}_{\rm pair} = -G\sum_{\xi,\eta>0}^{\xi\neq\eta}\hat{\beta}_{\xi+}^\dagger\hat{\beta}_{\xi-}^\dagger\hat{\beta}_{\eta-}\hat{\beta}_{\eta+}. \tag{17}$$

The idea of SLAP is to diagonalize the many-body Hamiltonian in a properly truncated MPC space with exact particle number [45]. One can diagonalize the cranking many-body Hamiltonian (14) in the MPC space constructed from the single-particle states either in the CDFT or in the cranking CDFT. The latter is expected to achieve the same accuracy with smaller MPC space.

Diagonalizing the one-body Hamiltonian $\hat{H}_0$ (16) in the bases $|\xi\alpha\rangle$ (11) and (12), one can obtain the single-particle Routhian $\varepsilon_{\mu\alpha}$ and the corresponding eigenstate $|\mu\alpha\rangle$ for each level μ with the signature α, namely,

$$\hat{H}_0 = \sum_{\mu\alpha}\varepsilon_{\mu\alpha}\hat{b}_{\mu\alpha}^\dagger\hat{b}_{\mu\alpha}, \quad |\mu\alpha\rangle = \sum_\xi C_{\mu\xi}(\alpha)|\xi\alpha\rangle. \tag{18}$$

From the real expansion coefficient $C_{\mu\xi}(\alpha)$, the transformation between the operators $\hat{b}_{\mu\alpha}^\dagger$ and $\hat{\beta}_{\xi\alpha}^\dagger$ can be expressed as

$$\hat{b}_{\mu\alpha}^\dagger = \sum_\xi C_{\mu\xi}(\alpha)\hat{\beta}_{\xi\alpha}^\dagger, \quad \hat{\beta}_{\xi\alpha}^\dagger = \sum_\mu C_{\mu\xi}(\alpha)\hat{b}_{\mu\alpha}^\dagger. \tag{19}$$

In the $|\mu\alpha\rangle$ basis, the pairing Hamiltonian $\hat{H}_{\rm pair}$ can be written as

$$\hat{H}_{\rm pair} = -G\sum_{\mu\mu'\nu\nu'}\sum_{\xi,\eta>0}^{\xi\neq\eta}C_{\mu\xi}(+)C_{\mu'\xi}(-)C_{\nu\eta}(-) \times C_{\nu'\eta}(+)\hat{b}_{\mu+}^\dagger\hat{b}_{\mu'-}^\dagger\hat{b}_{\nu-}\hat{b}_{\nu'+}. \tag{20}$$

From the single-particle Routhian $\varepsilon_{\mu\alpha}$ and the corresponding eigenstate $|\mu\alpha\rangle$ (briefly denoted by $|\mu\rangle$), the MPC $|i\rangle$ for an n-particle system can be constructed as [85]

$$|i\rangle = |\mu_1\mu_2\ldots\mu_n\rangle = \hat{b}_{\mu_1}^\dagger\hat{b}_{\mu_2}^\dagger\ldots\hat{b}_{\mu_n}^\dagger|0\rangle. \tag{21}$$

The parity π, signature α, and the corresponding configuration energy for each MPC are obtained from the occupied single-particle states.

The eigenstates for the cranking many-body Hamiltonian are obtained by diagonalization in the MPC space,

$$|\Psi\rangle = \sum_i C_i |i\rangle, \tag{22}$$

with C_i the expanding coefficients.

The occupation probability n_μ for state μ is

$$n_\mu = \sum_i |C_i|^2 P_{i\mu},\ P_{i\mu} = \begin{cases} 1, & |i\rangle \text{ contains } |\mu\rangle, \\ 0, & \text{otherwise.} \end{cases} \tag{23}$$

The occupation probabilities will be iterated back into the densities and currents in Eq. (5) to achieve self-consistency [44].

It is noted that for the total energy in CDFT (6), the pairing energy due to the pairing correlations should be taken into account, $E_{\text{pair}} = \langle\Psi|\hat{H}_{\text{pair}}|\Psi\rangle$.

III. NUMERICAL DETAILS

As mentioned before, the cranking many-body Hamiltonian (14) can be diagonalized in the MPC space constructed from the single-particle states either in the CDFT or in the cranking CDFT. The latter is expected to achieve the same accuracy with smaller MPC space.

In the following, the validity for diagonalizing the cranking many-body Hamiltonian (14) in MPC space constructed from the single-particle states in the cranking CDFT, namely cranking CDFT-SLAP, will be checked.

In the present cranking CDFT-SLAP calculations for ^{60}Fe, the point-coupling density functional PC-PK1 [79] is used in the particle-hole channel and the monopole pairing interaction is adopted in the particle-particle channel. The equation of motion (2) is solved by expanding the Dirac spinor in terms of the 3DHO bases (11) and (12) with 10 major shells. For both neutron and proton, the dimensions of the MPC space are chosen as 800, which correspond to the energy cutoffs $E_c \approx 12.1$ and ≈ 18.5 MeV, respectively. The effective pairing strengths are 0.8 MeV for both neutron and proton by reproducing the experimental odd-even mass differences. Increasing the number of major shells from 10 to 12, the change of the total energy is within 0.1%. Increasing the dimension of the MPC space from 800 to 1200 and adjusting the effective pairing strength accordingly, the change of the total energy is within 0.1%. In the present calculation, there is no free parameter.

The validity for cranking CDFT-SLAP at the rotational frequency $\hbar\omega = 0.0$ MeV is confirmed by reproducing the results in Ref. [44], indicating that the pairing correlations have been taken into account correctly.

The validity for cranking CDFT-SLAP is also checked against the TAC-CDFT [25] calculation with the pairing correlations switching off. The neutron single-particle Routhian and the alignment along the rotational axis $J_x = \langle\Psi|\hat{J}_x|\Psi\rangle$ as functions of the rotational frequency in ^{60}Fe calculated by the cranking CDFT-SLAP are shown in Fig. 1, in comparison with the TAC-CDFT [25] calculations with tilted angle $\theta = 0^\circ$. Satisfactory agreement is found with the differences less than 10^{-4} MeV for the neutron single-particle Routhian and $10^{-4}\hbar$ for J_x.

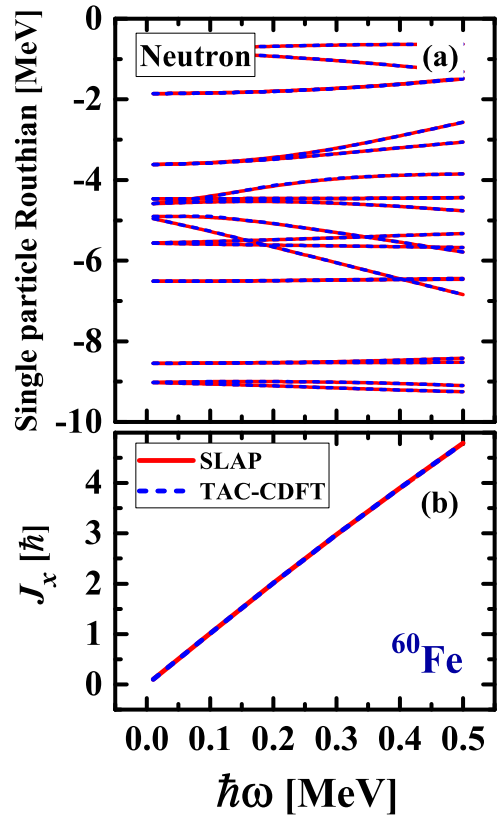

FIG. 1. The neutron single-particle Routhian (a) and the alignment along the rotational axis J_x (b) as functions of the rotational frequency in ^{60}Fe calculated by the cranking CDFT-SLAP with PC-PK1 [79], in comparison with the TAC-CDFT [25] calculations with tilted angle $\theta = 0^\circ$.

IV. RESULTS AND DISCUSSION

Three rotational bands of the neutron-rich nucleus ^{60}Fe have been observed in Ref. [76], including the yrast band with positive parity (labeled as band A) and two negative-parity signature partner bands with similar intensity starting from 6^- and 5^- states (labeled as bands B and C), respectively. As both parity and signature are good quantum numbers, the cranking many-body Hamiltonian (14) can be diagonalized in the corresponding MPC space. The yrast bands thus obtained for different parity and signature are compared with the observed bands A, B, and C.

A. Energy spectra and $I - \omega$ relations

At a given rotational frequency, the eigenstate $|\Psi\rangle$ of the cranking many-body Hamiltonian (14) can be obtained by diagonalization in the MPC space. By adding the pairing energy $E_{\text{pair}} = \langle\Psi|\hat{H}_{\text{pair}}|\Psi\rangle$ to Eq. (6), the total energy of the system can be obtained. The corresponding spin I can be obtained through $J_x = \langle\Psi|\hat{J}_x|\Psi\rangle = \sqrt{I(I+1)}$.

In Fig. 2, the total energies and the rotational frequencies are shown as functions of the spin for the positive-parity band

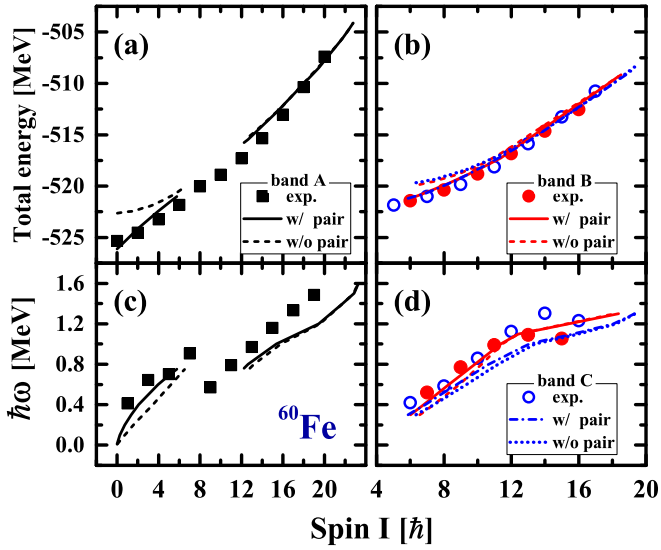

FIG. 2. The total energies (a) and (b) and the rotational frequencies (c) and (d) as functions of the spin for the positive-parity band A and negative-parity signature partner bands B and C in ^{60}Fe calculated by the cranking CDFT-SLAP with and without pairing, in comparison with the data available [76].

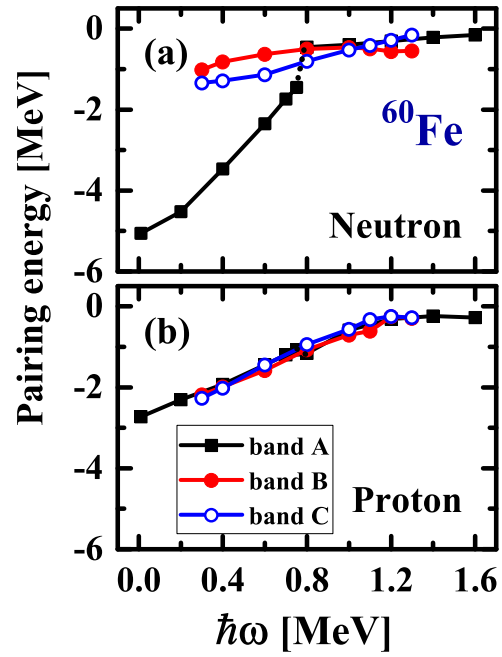

FIG. 3. The pairing energies as functions of the rotational frequency for neutron (a) and proton (b) in the positive-parity band A and negative-parity signature partner bands B and C.

A and negative-parity signature partner bands B and C in ^{60}Fe calculated by the cranking CDFT-SLAP with and without pairing correlations, in comparison with the available data.

In Figs. 2(a) and 2(b), the cranking CDFT-SLAP calculations well reproduce the energy spectra for bands A, B, and C without introducing any *ad hoc* parameters. By switching off the pairing correlations, the deviations appear for the low-spin regions, in particular, for band A.

In Figs. 2(c) and 2(d), the cranking CDFT-SLAP calculations well reproduce the $I - \omega$ relations including the band crossings for bands A, B, and C. By switching off the pairing correlations, the deviations appear for the low-spin region for band A.

In Fig. 3, the pairing energies as functions of the rotational frequency for neutron and proton are shown for the positive-parity band A and negative-parity signature partner bands B and C. Generally, the pairing energies decrease with rotational frequency, and there is no sharp transition where the pairing field goes to zero but rather a more continuous transition as rotational frequency is increased. This is similar to what is obtained when particle number projection is employed.

For neutron, as seen in Fig. 3(a), the pairing energy in band A changes rapidly from ≈ -5.0 MeV near the bandhead to ≈ -1.5 MeV at $\hbar\omega \approx 0.75$ MeV, where the band crossing occurs. After band crossing, it changes similarly as bands B and C. In comparison with band A, the pairing energies in bands B and C are relatively small because the neutron pair in the $1f_{5/2,3/2}$ orbitals is broken (see the following).

For proton, as seen in Fig. 3(b), the pairing energies change smoothly and similarly as functions of rotational frequency for bands A, B, and C, which suggest that the proton configurations are the same. In comparison with the neutron, the suppressed pairing correlations for proton are due to the lower level density (see the following).

The excellent agreements with the observed energy spectra and $I - \omega$ relations indicate that the cranking CDFT-SLAP correctly treats the pairing correlations and mean-field involved. From the calculations, one can pin down the corresponding configurations and examine the mechanism for band crossing.

B. Single-particle Routhians

To explore the mechanism of the observed band crossings, in Figs. 4 and 5, the single-particle Routhians as functions of the rotational frequency for bands A and B are shown.

As shown in Fig. 4(a), the occupied neutron orbitals for band A change around $\hbar\omega \approx 0.75$ MeV. A discontinuity is observed in the neutron single-particle Routhians. Using the single-particle level tracking technique [15], the levels with the largest overlap (>0.9) before and after the discontinuity are connected. It is found that the last two occupied neutrons change from the $1f_{5/2}$ signature partners to the $1g_{9/2}$ signature partners. The occupation probabilities of the two $1g_{9/2}$ signature partners change from less than 10^{-1} at $\hbar\omega = 0.6$ MeV [cf. Fig. 4(b)] to nearly 1 at $\hbar\omega = 1.2$ MeV [cf. Fig. 4(c)]. This configuration change for band A results from the rapid decrease of the neutron $1g_{9/2}$ orbitals with rotational frequency. For proton in band A, as shown in Figs. 4(d)–4(f), the occupation probabilities change smoothly. The discontinuity in the proton single-particle Routhians results from the change of the mean field due to the neutron band crossing around $\hbar\omega \approx 0.75$ MeV. Hence, the configuration for band A after band crossing can be assigned as $\nu(1g_{9/2})^2(1f_{5/2})^{-2}$, which is in consistent with the assignment by the shell model [76] and the projected shell model [77].

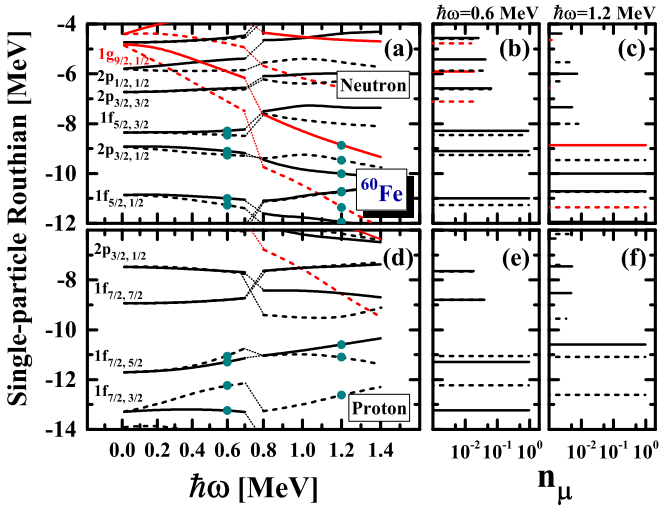

FIG. 4. The neutron (a) and proton (d) single-particle Routhians as functions of the rotational frequency for band A in ^{60}Fe. Each orbital is labeled by the corresponding spherical quantum number of its main component. The positive-parity (negative-parity) levels are denoted by red or light gray (black) lines. The signature $\alpha = +1/2$ $(-1/2)$ levels are denoted by solid (dashed) lines. The solid circles denote the occupied orbitals, and the corresponding occupation probabilities n_μ are given in the right two columns.

For neutron in band B, as shown in Figs. 5(a)–5(c), the occupation probabilities change smoothly, and the neutron configuration can be assigned as $\nu(g_{9/2})^1(1f_{5/2})^{-1}$. For proton in band B, as shown in Figs. 5(d)–5(f), a pseudocrossing is seen between the $1f_{7/2,5/2}$ and the $1f_{5/2,1/2}$ orbitals at $\hbar\omega \approx 1.1$ MeV. The occupation probability of the proton $1f_{5/2,1/2}$ orbital change from about 10^{-2} to nearly 1, while that of the $1f_{7/2,5/2}$ changes from nearly 1 to less than 10^{-2}.

As band C is the signature partner of band B, its detailed discussions of the neutron and proton single-particle Routhians and occupation probabilities are not shown here.

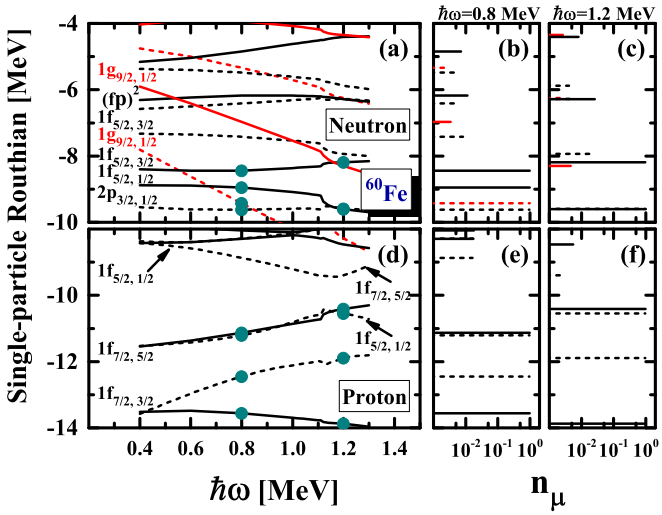

FIG. 5. Same as Fig. 4 but for band B.

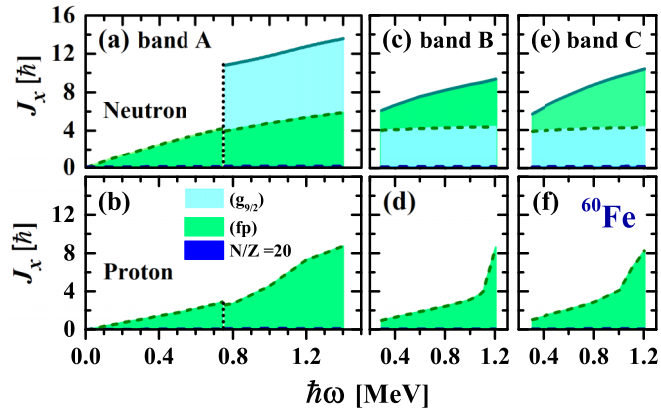

FIG. 6. The contributions from the neutron and proton $1g_{9/2}$, (fp), and $N/Z = 20$ shells to the angular momentum J_x as functions of the rotational frequency for the positive-parity band A [(a), (b)] and negative-parity signature partner bands B [(c), (d)] and C [(e), (f)].

C. Angular momentum components

In the present fully self-consistent and microscopic cranking CDFT-SLAP calculation, the angular momentum can be calculated from the single neutron and proton orbitals. In Fig. 6, the contributions from the neutron and proton $1g_{9/2}$, (fp), and $N/Z = 20$ shells to the angular momentum J_x for bands A, B, and C are shown.

For all bands, both the $N = 20$ and $Z = 20$ shells do not contribute (core ^{40}Ca is inert), and only nucleons in the (fp) shells and $1g_{9/2}$ orbitals contribute.

For neutron in band A, as shown in Fig. 6(a), the contributions from the (fp) shells change smoothly. After band crossing at $\hbar\omega \approx 0.75$ MeV, the contributions from the $1g_{9/2}$ orbitals are switched on, which produce a dramatic change around $6\hbar$. For proton, as shown in Fig. 6(b), the contributions are mainly from the (fp) shells, which have a kink around band crossing but change smoothly before and after.

For neutron in band B, as shown in Fig. 6(c), the contributions from the (fp) shells change smoothly. In contrast, the contribution from the $1g_{9/2}$ orbital stays nearly unchanged $(\approx 4\hbar)$ due to its high-j, low-Ω character. For proton, as shown in Fig. 6(d), the contributions from the (fp) shells increase smoothly with the rotational frequency but much more quickly after $\hbar\omega = 1.1$ MeV. This faster increase is due to the pseudocrossing between the orbitals $1f_{7/2,5/2}$ and $1f_{5/2,1/2}$, as shown in Fig. 5(b).

For neutron and proton in band C, as shown in Figs. 6(e) and 6(f), the contributions of the angular momenta can be explained similarly as its signature partner band B.

D. Shape evolution with rotation

To investigate the shape evolution with rotation in ^{60}Fe, the total Routhian surfaces (TRSs) for the positive-parity band A at $\hbar\omega = 0.0, 0.4, 0.8$, and 1.2 MeV, and negative-parity signature partner bands B and C at $\hbar\omega = 0.4, 0.8$, and 1.2 MeV are shown in Fig. 7. The evolution of the deformation parameters β and γ with the rotational frequency are shown in Figs. 7(e), 7(i), and

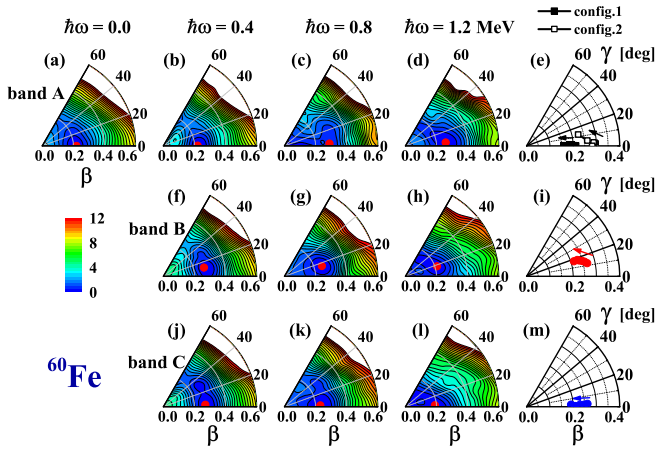

FIG. 7. The total Routhian surfaces for the positive-parity band A [(a)–(d)] at $\hbar\omega = 0.0, 0.4, 0.8$, and 1.2 MeV, and negative-parity bands B [(f)–(h)] and C [(j)–(l)] at $\hbar\omega = 0.4, 0.8$ and 1.2 MeV. The red dot in the energy surface denotes the minimum. The energy difference between the neighboring contour lines is 0.5 MeV. The evolutions of the deformation parameters β and γ with the rotational frequency are shown in panels (e), (i), and (m). For band A, the configurations before and after the band crossing are denoted as config. 1 and config. 2, respectively.

7(m). For band A, the configurations before and after the band crossing are denoted as config. 1 and config. 2, respectively.

For band A, as mentioned before, the band crossing occurs at $\hbar\omega \approx 0.75$ MeV. Before the band crossing, the deformation parameters (β, γ) of the TRS minimum at $\hbar\omega = 0.0$ MeV are around $(0.21, 0^\circ)$. With the increase of the rotational frequency, the deformation parameter β decreases but the potential becomes more rigid. After the band crossing, the deformation parameters of the TRS minimum at $\hbar\omega = 0.8$ MeV are around $(0.29, 0^\circ)$. The dramatic change of the β results from the deformation driving effect of the neutron $1g_{9/2}$ orbital. With the increase of the rotational frequency, the deformation parameter β decreases but γ increases. The potential becomes more rigid with β but softer with γ. The deformation parameters of the TRS minimum at $\hbar\omega = 1.4$ MeV are around $(0.23, 12^\circ)$.

For band B, the deformation parameters of the TRS minimum at $\hbar\omega = 0.4$ MeV are around $(0.27, 12^\circ)$. With the increase of the rotational frequency, the deformation parameter β decreases but γ increases, and the potential becomes softer. The deformation parameters of the TRS minimum at $\hbar\omega = 1.2$ MeV are around $(0.21, 18^\circ)$.

Although bands B and C are signature partner bands, there is no triaxial deformation in band C. With the increase of the rotational frequency, the deformation of the TRS minimum decreases from $\beta = 0.27$ at $\hbar\omega = 0.4$ MeV to $\beta = 0.19$ at $\hbar\omega = 1.2$ MeV.

V. SUMMARY

In summary, the shell-model-like approach is implemented to treat the cranking many-body Hamiltonian based on the covariant density functional theory including pairing correlations with exact particle number conservation, referred to as cranking CDFT-SLAP. The self-consistency is achieved by iterating the single-particle occupation probabilities back to the densities and currents.

As an example, the rotational spectra observed in the neutron-rich nucleus ^{60}Fe, including the positive-parity band A and two negative-parity signature partner bands B and C, are investigated and analyzed. Without introducing any *ad hoc* parameters, the bandheads, the rotational spectra, and the relations between the angular momentum and rotational frequency for bands A, B, and C are well reproduced. It is found that pairing correlations are important to describe these quantities, especially for the low-spin part. By examining the single-particle Routhians, the occupation probabilities, and the contributions from the $1g_{9/2}$, (fp), and $N/Z = 20$ shells to the angular momentum, the mechanisms of the band crossings are analyzed and discussed in detail. It is found that for band A, the band crossing is due to the change of the last two occupied neutrons from the $1f_{5/2}$ signature partners to the $1g_{9/2}$ signature partners. For the two negative-parity signature partner bands B and C, the band crossings are due to the pseudocrossing between the $1f_{7/2,5/2}$ and the $1f_{5/2,1/2}$ orbitals. The shape evolutions with rotation are investigated from the total Routhian surfaces. For band A, the deformation parameter β decreases with rotational frequency before and after the band crossing. A dramatic change of β is observed around the band crossing at the frequency $\hbar\omega \approx 0.75$ MeV, which results from the deformation driving effect of the neutron $1g_{9/2}$ orbital. For band B, the deformation evolves from $(0.27, 12^\circ)$ at $\hbar\omega = 0.4$ MeV to $(0.21, 18^\circ)$ at $\hbar\omega = 1.2$ MeV. For band C, there is no triaxial deformation, and the deformation evolves from $\beta = 0.27$ at $\hbar\omega = 0.4$ MeV to $\beta = 0.19$ at $\hbar\omega = 1.2$ MeV.

ACKNOWLEDGMENTS

Z.S. is indebted to Fangqi Chen, Jing Peng, Zhengxue Ren, Yakun Wang, Yuanyuan Wang, Xinhui Wu, Binwu Xiong, and Pengwei Zhao for the fruitful discussions. This work was partly supported by the Chinese Major State 973 Program (Grant No. 2013CB834400); the National Natural Science Foundation of China (NSFC) under Grants No. 11335002, No. 11505058, No. 11621131001, No. 11775026, No. 11375015, and No. 11461141002; and the Deutsche Forschungsgemeinschaft (DFG) and NSFC through funds provided to the Sino-German CRC 110 "Symmetries and the Emergence of Structure in QCD."

[1] P. J. Twin, B. M. Nyakó, A. H. Nelson, J. Simpson, M. A. Bentley, H. W. Cranmer-Gordon, P. D. Forsyth, D. Howe, A. R. Mokhtar, J. D. Morrison *et al.*, Phys. Rev. Lett. **57**, 811 (1986).

[2] P. Ring, Prog. Part. Nucl. Phys. **37**, 193 (1996).

[3] I. Tanihata, H. Hamagaki, O. Hashimoto, Y. Shida, N. Yoshikawa, K. Sugimoto, O. Yamakawa, T. Kobayashi, and N. Takahashi, Phys. Rev. Lett. **55**, 2676 (1985).

[4] J. Meng and P. Ring, Phys. Rev. Lett. **77**, 3963 (1996).

[5] J. Meng and P. Ring, Phys. Rev. Lett. **80**, 460 (1998).
[6] J. Meng, H. Toki, S.-G. Zhou, S. Q. Zhang, W. H. Long, and L. S. Geng, Prog. Part. Nucl. Phys. **57**, 470 (2006).
[7] J. Meng and S.-G. Zhou, J. Phys. G **42**, 093101 (2015).
[8] A. Ozawa, T. Kobayashi, T. Suzuki, K. Yoshida, and I. Tanihata, Phys. Rev. Lett. **84**, 5493 (2000).
[9] S. Frauendorf, J. Meng, and J. Reif, in *Proceedings of the Conference on Physics From Large γ-Ray Detector Arrays*, edited by M. A. Deleplanque (University of California, Berkeley, 1994), p. 52.
[10] R. M. Clark, S. J. Asztalos, G. Baldsiefen, J. A. Becker, L. Bernstein, M. A. Deleplanque, R. M. Diamond, P. Fallon, I. M. Hibbert, H. Hübel *et al.*, Phys. Rev. Lett. **78**, 1868 (1997).
[11] S. Frauendorf, Rev. Mod. Phys. **73**, 463 (2001).
[12] J. Meng, J. Peng, S. Q. Zhang, and P. W. Zhao, Front. Phys. **8**, 55 (2013).
[13] S. Frauendorf and J. Meng, Nucl. Phys. A **617**, 131 (1997).
[14] K. Starosta, T. Koike, C. Chiara, D. Fossan, D. LaFosse, A. Hecht, C. Beausang, M. Caprio, J. Cooper, R. Krücken *et al.*, Phys. Rev. Lett. **86**, 971 (2001).
[15] J. Meng, J. Peng, S. Q. Zhang, and S.-G. Zhou, Phys. Rev. C **73**, 037303 (2006).
[16] A. D. Ayangeakaa, U. Garg, M. D. Anthony, S. Frauendorf, J. T. Matta, B. K. Nayak, D. Patel, Q. B. Chen, S. Q. Zhang, P. W. Zhao *et al.*, Phys. Rev. Lett. **110**, 172504 (2013).
[17] I. Kuti, Q. B. Chen, J. Timár, D. Sohler, S. Q. Zhang, Z. H. Zhang, P. W. Zhao, J. Meng, K. Starosta, T. Koike *et al.*, Phys. Rev. Lett. **113**, 032501 (2014).
[18] C. Liu, S. Y. Wang, R. A. Bark, S. Q. Zhang, J. Meng, B. Qi, P. Jones, S. M. Wyngaardt, J. Zhao, C. Xu *et al.*, Phys. Rev. Lett. **116**, 112501 (2016).
[19] H. Z. Liang, J. Meng, and S.-G. Zhou, Phys. Rep. **570**, 1 (2015).
[20] J. Meng, *Relativistic Density Functional for Nuclear Structure* (World Scientific, Singapore, 2015).
[21] W. Koepf and P. Ring, Nucl. Phys. A **493**, 61 (1989).
[22] H. Madokoro, J. Meng, M. Matsuzaki, and S. Yamaji, Phys. Rev. C **62**, 061301 (2000).
[23] W. Koepf and P. Ring, Nucl. Phys. A **511**, 279 (1990).
[24] J. Peng, J. Meng, P. Ring, and S. Q. Zhang, Phys. Rev. C **78**, 024313 (2008).
[25] P. W. Zhao, S. Q. Zhang, J. Peng, H. Z. Liang, P. Ring, and J. Meng, Phys. Lett. B **699**, 181 (2011).
[26] P. W. Zhao, Phys. Lett. B **773**, 1 (2017).
[27] J. König and P. Ring, Phys. Rev. Lett. **71**, 3079 (1993).
[28] A. V. Afanasjev, J. König, and P. Ring, Nucl. Phys. A **608**, 107 (1996).
[29] L. F. Yu, P. W. Zhao, S. Q. Zhang, P. Ring, and J. Meng, Phys. Rev. C **85**, 024318 (2012).
[30] P. W. Zhao, J. Peng, H. Z. Liang, P. Ring, and J. Meng, Phys. Rev. Lett. **107**, 122501 (2011).
[31] P. W. Zhao, J. Peng, H. Z. Liang, P. Ring, and J. Meng, Phys. Rev. C **85**, 054310 (2012).
[32] P. W. Zhao, N. Itagaki, and J. Meng, Phys. Rev. Lett. **115**, 022501 (2015).
[33] A. Bohr and B. R. Mottelson, *Nuclear Structure* (Benjamin, New York, 1975), Vol. 2.
[34] P. Ring and P. Schuck, *The Nuclear Many-Body Problem* (Springer-Verlag, Berlin, 1980).
[35] A. V. Afanasjev, J. König, and P. Ring, Phys. Rev. C **60**, 051303 (1999).
[36] Z. M. Niu, Y. F. Niu, H. Z. Liang, W. H. Long, T. Nikšić, D. Vretenar, and J. Meng, Phys. Lett. B **723**, 172 (2013).
[37] P. W. Zhao, S. Q. Zhang, and J. Meng, Phys. Rev. C **92**, 034319 (2015).
[38] Z. M. Niu, Y. F. Niu, H. Z. Liang, W. H. Long, and J. Meng, Phys. Rev. C **95**, 044301 (2017).
[39] B. R. Mottelson and J. G. Valatin, Phys. Rev. Lett. **5**, 511 (1960).
[40] K. Dietrich, H. J. Mang, and J. H. Pradal, Phys. Rev. **135**, B22 (1964).
[41] M. Anguiano, J. Egido, and L. Robledo, Nucl. Phys. A **696**, 467 (2001).
[42] M. V. Stoitsov, J. Dobaczewski, R. Kirchner, W. Nazarewicz, and J. Terasaki, Phys. Rev. C **76**, 014308 (2007).
[43] J. M. Yao, K. Hagino, Z. P. Li, J. Meng, and P. Ring, Phys. Rev. C **89**, 054306 (2014).
[44] J. Meng, J. Y. Guo, L. Liu, and S. Q. Zhang, Front. Phys. China. **1**, 38 (2006).
[45] J. Y. Zeng and T. S. Cheng, Nucl. Phys. A **405**, 1 (1983).
[46] J. Y. Zeng, Y. A. Lei, T. H. Jin, and Z. J. Zhao, Phys. Rev. C **50**, 746 (1994).
[47] S. X. Liu, J. Y. Zeng, and E. G. Zhao, Phys. Rev. C **66**, 024320 (2002).
[48] X. T. He, S. X. Liu, S. Y. Yu, J. Y. Zeng, and E. G. Zhao, Euro. Phys. J. A **23**, 217 (2005).
[49] X. Wu, Z. H. Zhang, J. Y. Zeng, and Y. A. Lei, Phys. Rev. C **83**, 034323 (2011).
[50] Z. H. Zhang, P. W. Zhao, J. Meng, J. Y. Zeng, E. G. Zhao, and S.-G. Zhou, Phys. Rev. C **87**, 054314 (2013).
[51] Z. H. Zhang, Phys. Rev. C **94**, 034305 (2016).
[52] S. X. Liu, J. Y. Zeng, and L. Yu, Nuc. Phys. A **735**, 77 (2004).
[53] Z. H. Zhang, X. Wu, Y. A. Lei, and J. Y. Zeng, Nucl. Phys. A **816**, 19 (2009).
[54] Z. H. Zhang, Y. A. Lei, and J. Y. Zeng, Phys. Rev. C **80**, 034313 (2009).
[55] B. H. Li, Z. H. Zhang, and Y. A. Lei, Chin. Phys. C **37**, 014101 (2013).
[56] Y. C. Li and X. T. He, Sci. China Phys. Mech. **59**, 672011 (2016).
[57] Z. H. Zhang, Nucl. Phys. A **949**, 22 (2016).
[58] Z. H. Zhang, J. Meng, E. G. Zhao, and S.-G. Zhou, Phys. Rev. C **87**, 054308 (2013).
[59] X. T. He, Z. Z. Ren, S. X. Liu, and E. G. Zhao, Nucl. Phys. A **817**, 45 (2009).
[60] Z. H. Zhang, J. Y. Zeng, E. G. Zhao, and S.-G. Zhou, Phys. Rev. C **83**, 011304 (2011).
[61] Z. H. Zhang, X. T. He, J. Y. Zeng, E. G. Zhao, and S.-G. Zhou, Phys. Rev. C **85**, 014324 (2012).
[62] L. Liu, Z. H. Zhang, and P. W. Zhao, Phys. Rev. C **92**, 044304 (2015).
[63] H. Molique and J. Dudek, Phys. Rev. C **56**, 1795 (1997).
[64] X. M. Fu, F. R. Xu, J. C. Pei, C. F. Jiao, Y. Shi, Z. H. Zhang, and Y. A. Lei, Phys. Rev. C **87**, 044319 (2013).
[65] N. Pillet, P. Quentin, and J. Libert, Nucl. Phys. A **697**, 141 (2002).
[66] W. Y. Liang, C. F. Jiao, Q. Wu, X. M. Fu, and F. R. Xu, Phys. Rev. C **92**, 064325 (2015).
[67] R. Richardson and N. Sherman, Nucl. Phys. **52**, 221 (1964).
[68] F. Pan, J. Draayer, and W. Ormand, Phys. Lett. B **422**, 1 (1998).
[69] A. Volya, B. Brown, and V. Zelevinsky, Phys. Lett. B **509**, 37 (2001).
[70] L. Y. Jia, Phys. Rev. C **88**, 044303 (2013).

[71] L. Y. Jia, Phys. Rev. C **88**, 064321 (2013).
[72] W. C. Chen, J. Piekarewicz, and A. Volya, Phys. Rev. C **89**, 014321 (2014).
[73] E. K. Warburton, J. W. Olness, A. M. Nathan, J. J. Kolata, and J. B. McGrory, Phys. Rev. C **16**, 1027 (1977).
[74] E. B. Norman, C. N. Davids, and C. E. Moss, Phys. Rev. C **18**, 102 (1978).
[75] A. N. Wilson, C. W. Beausang, N. Amzal, D. E. Appelbe, S. Asztalos, P. A. Butler, R. M. Clark, P. Fallon, and A. O. Macchiavelli, Eur. Phys. J. A **9**, 183 (2000).
[76] A. N. Deacon, S. J. Freeman, R. V. F. Janssens, M. Honma, M. P. Carpenter, P. Chowdhury, T. Lauritsen, C. J. Lister, D. Seweryniak, J. F. Smith *et al.*, Phys. Rev. C **76**, 054303 (2007).
[77] Y. Sun, Y. C. Yang, H. L. Liu, K. Kaneko, M. Hasegawa, and T. Mizusaki, Phys. Rev. C **80**, 054306 (2009).
[78] T. Togashi, N. Shimizu, Y. Utsuno, T. Otsuka, and M. Honma, Phys. Rev. C **91**, 024320 (2015).
[79] P. W. Zhao, Z. P. Li, J. M. Yao, and J. Meng, Phys. Rev. C **82**, 054319 (2010).
[80] K. Kaneko, M. Nakano, and M. Matsuzaki, Phys. Lett. B **317**, 261 (1993).
[81] W. Koepf and P. Ring, Phys. Lett. B **212**, 397 (1988).
[82] J. Dobaczewski and J. Dudek, Comput. Phys. Commun. **102**, 166 (1997).
[83] J. M. Yao, H. Chen, and J. Meng, Phys. Rev. C **74**, 024307 (2006).
[84] T. Nikšić, Z. P. Li, D. Vretenar, L. Próchniak, J. Meng, and P. Ring, Phys. Rev. C **79**, 034303 (2009).
[85] J. Y. Zeng, T. H. Jin, and Z. J. Zhao, Phys. Rev. C **50**, 1388 (1994).